Rare Metal Materials and Engineering
Volume 54, Issue 8, August 2025
Available online at www.rmme.ac.cn

Science Press

Cite this article as: Chao Rui, Ye Borui. Erosion Resistance and Damage Evolution of Ti-doped Ta_2O_5 High-Transmittance Coatings[J]. Rare Metal Materials and Engineering, 2025, 54(08): 1988-1996. DOI: https://doi.org/10.12442/j.issn.1002-185X.20240563.

ARTICLE

Erosion Resistance and Damage Evolution of Ti-doped Ta_2O_5 High-Transmittance Coatings

Chao Rui[1,2], Ye Borui[3]

[1] School of Mechatronics Engineering, Henan University of Science and Technology, Luoyang 471003, China; [2] Henan Key Laboratory for Machinery Design and Transmission System, Luoyang 471003, China; [3] School of Mechanical Engineering, Hefei University of Technology, Hefei 230009, China

Abstract: To verify the wear resistance and erosion resistance of Ti-doped Ta_2O_5 coating (TTO), a series of TTOs were prepared by magnetron sputtering technology by controlling the power of the Ti target. The change of growth structure, microstructure, and tribological properties of TTOs with Ti target power was studied. After the erosion test, the variation of erosion damage behavior of TTOs with mechanical properties under different erosion conditions was further studied. The results show that the TTOs eliminate the roughness, voids, and defects in the material due to the mobility of the adsorbed atoms during the growth process, and a flat and dense smooth surface is obtained. Tribological tests show that the TTOs are mainly characterized by plastic deformation and microcrack wear mechanism. Higher Ti target power can improve the wear resistance of TTOs. Erosion test results reveal that the impact crater, furrow, micro-cutting, brittle spalling, and crack formation are the main wear mechanisms of the TTOs samples under erosion conditions.

Key words: Ti-Ta_2O_5 coatings; microstructure; tribological properties; erosion behavior; damage law

1 Introduction

As a clean, sustainable, and widely distributed renewable energy source, solar energy is the main technology driving energy transformation to mitigate climate change[1–3]. Due to the scalable nature and ease of distributed deployment of photovoltaic (PV) power generation, its potential is enormous[4]. PV power generation has increased significantly and has become the main source of electricity in clean energy[5]. PV power generation has fundamentally increased the importance of renewable energy[6–7]. Currently, PV power generation accounts for 6.3% and 1.7% of global installed capacity and power generation, respectively[5]. At present, the most advanced technologies for converting solar radiation into electrical energy are PV solar panels and concentrating solar thermal (CSP) systems[8–10].

The desert areas, characterized by abundant solar resources and low-cost land availability, are ideal for constructing large-scale PV power stations[11]. The latest research on climate change shows that the frequency of dust storms in desert areas has increased significantly, posing severe threats to solar energy collection systems, especially PV systems[12]. The transparent glass cover plate in the PV power generation system module is the top layer, which is designed to protect the PV cells from the impact of dust erosion. Debris and sand in desert areas can cause erosion and wear on the surface of PV panels under the action of dust storms. Erosion and wear of the PV panel surface caused by sand erosion and the cleaning process to remove deposited particles may result in a decrease in optical transmittance of glass cover plates or even permanent loss[13–15]. The damage to the surface of the glass protective cover from sand particles depends on the intensity of the dust storm, which is essentially related to the wind speed, size and shape of the incident particles, and dust storm duration[16–18]. The reduction in photoelectric conversion efficiency, often leading to system failure, is a major problem in the desert environments. The accumulation and erosion of dust particles on the surface of PV modules are the main factors for the overall performance degradation of PVs[19–21].

Received date: August 29, 2024
Corresponding author: Chao Rui, Ph. D., School of Mechatronics Engineering, Henan University of Science and Technology, Luoyang 471003, P. R. China, E-mail: chaoruibr@163.com

To maintain the system efficiency, it is necessary to protect the outer surface of the glass cover plate in the PV module, which is usually made of transparent glass[14]. Therefore, transparent glass is required not only to ensure high transparency of solar radiation, but also to provide the necessary mechanical properties to protect the surface of the PV system from harsh environments[22].

To protect PV panels from sand erosion damage, high-performance coatings have emerged as a critical choice[23–24]. When eroded by irregular gravel, the coatings should be harder than the erosion agent, along with stronger adhesion and a dense microstructure to improve the corrosion resistance[25]. There have been many studies on erosion-resistant coatings. Naveed et al[26] studied the effect of vacuum-annealed Ti_2AlC MAX phase coating on the high-speed particle erosion resistance of Ti6242 alloy surfaces, demonstrating their potential as an protection medium for engine components under similar erosion conditions. Zambrano-Mera et al[27] discussed the effect of ZrO_2 doping on the microstructure, optical, and mechanical properties of multi-layer TiO_2/SiO_2 coatings, aiming to synergistically enhance the optical and mechanical properties of multi-layer coatings. Wiesinger et al[28] conducted artificial dust storm tests on four anti-reflection (AR) coatings deposited on borosilicate glass and evaluated their corrosion resistance. Metallic materials typically exhibit excellent ductility coupled with high resistance to plastic deformation, especially Ti, which has been widely used due to its high strength and low elastic modulus. The alloying of Ti and Ta with similar atomic size can improve the passivation performance of the coatings[29]. However, the effect of Ti doping on the erosion resistance of Ta_2O_5 coatings has seldom been studied. To prepare Ti-doped Ta_2O_5 coating (TTO) with excellent erosion resistance, it is necessary to study the effects of different Ti contents on the microstructure and erosion resistance of TTOs.

In this research, high-transmittance TTO was prepared by magnetron sputtering technology. The microstructure, mechanical, and tribological properties of TTOs were investigated. The erosion wear resistance of TTOs was studied by a self-designed fully enclosed micro-particle erosion tester. In addition, the erosion resistance and erosion damage evolution process of TTOs were analyzed by changing the wind speed, particle flow rate, and erosion angle. Finally, the erosion wear mechanism of TTOs under different erosion conditions was revealed by scanning electron microscope (SEM) and energy dispersive spectrometer (EDS). The study on the mechanical properties and erosion resistance of TTOs provides insights for predicting the durability and efficiency of the glass cover plates in solar panels as protective coatings.

2 Experiment

2.1 Deposition of TTOs

The films were deposited via RF-DC magnetron co-sputtering using Ta_2O_5 and Ti targets with a size of Φ50 mm× 3 mm and purity>99.9% by JGP045CA RF sputtering system. The back-bottom vacuum was pumped to below 5×10^{-4} Pa, the deposition pressure was 0.8 Pa, and the target-substrate distance was 120 mm. Because the PV power generation system uses transparent glass as a protective cover, high-transparent glass was also selected as the substrate during the experiment. The substrates were highly transparent quartz glasses and silicon substrates (Si 100). Si wafer was selected as the substrate to obtain the coating cross-section more conveniently and analyze the microstructure. The substrates were ultrasonically cleaned with acetone, anhydrous ethanol, and deionized water for 10 min using SCIENTZ-450 (Xinzhi Freeze-drying Equipment Co., Ltd) equipment before deposition, dried with compressed air, and prepared for use. Pre-sputtering by glow discharge was carried out for 10 min to obtain a clean target surface before deposition of the film, and the substrates were supported on a rotational base with a speed of 10 r/min. The Ti-Ta_2O_5 thin films were deposited at different sputtering powers. Table 1 shows the preparation parameters of the coatings.

2.2 Sand erosion experiment

The actual installation environment of PV panels was analyzed. According to ASTM-G76 standard[16,25], the erosion resistance of TTOs in a wind-sand environment was simulated through the self-designed and fully enclosed micro-particle erosion testing machine. The wind speed range of the device was 0–25 m/s, the sample scaffold could be freely adjusted from 0° to 90°, and the particle flow was controllable. The erosion test principle is shown in Fig. 1a. Quartz sand with a

Table 1 Deposition parameters of the TTOs

Sample	Target power/W		Flow of Ar/ mL·min^{-1}	Deposition pressure/Pa
	Ti (DC)	Ta_2O_5 (RF)		
S1	30	120	40	0.8
S2	40	120		
S3	50	120		
S4	60	120		

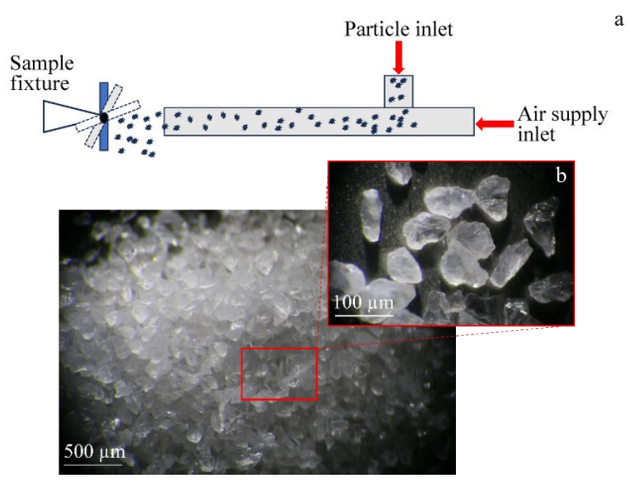

Fig.1 Erosion test principle (a) and erosion particle morphologies of TTOs (b)

particle size range of 80–160 μm was used for the erosion test. The shape of quartz sand was extremely irregular, with sharp edges and corners, as shown in Fig. 1b. All tests were conducted at room temperature. Before and after the test, the samples were ultrasonically cleaned for 5 min to remove the residual gravel. The coating samples S1 and S2 show high light transmittance. Specifically, in the wavelength range of 220–850 nm, the transmittance of the coatings samples S1 and S2 fluctuates between 72% and 88%. The maximum transmittance of the coating samples S1 and S2 reaches approximately 93.31% and 90.93%, respectively. Moreover, in the wavelength range of 220–850 nm, the reflectivity of the coating samples S1 and S2 is less than 25%. The band gaps of S1 and S2 are 3.98 and 3.76 eV, respectively. Corresponding research has been done in Ref. [21]. Therefore, this study mainly focused on the erosion test of coating samples S1 and S2. The specific parameters for particle erosion test of TTOs are shown in Table 2.

2.3 Morphology characterization of TTOs before and after erosion

Microstructure and surface structure of TTOs before and after the erosion test were analyzed. The nanostructure of TTOs was obtained by high-resolution transmission electron microscope (TEM, JEM-F200(URP)) at an accelerated voltage of 200 kV. The state of TTOs before and after erosion test was characterized by SEM (Zeiss Sigma 300), equipped with EDS, and atomic force microscope (AFM, Bruker Dimension Icon). A nanoindentation tester (ZDT075-075) was used to apply a load of 25 mN, ensuring that the indentation depth did not exceed 10% of the film thickness. The microhardness (*H*) and elastic modulus (*E*) of the film were obtained. The material high-frequency linear super-smooth testing machine (RTEC MFT-5000) was used. A GCr15 steel ball with a diameter of 5 mm was used as the friction partner. The reciprocating friction test was conducted with a load of 0.5 N, a reciprocating distance of 6 mm, and a frequency of 20 Hz/s at room temperature. The failure mechanism and wear traces of the TTOs were characterized by SEM.

Table 2 Erosion test parameters for coating samples S1 and S2

Wind speed/m·s^{-1}	Angle/(°)	Granular flux//g·s^{-1}	Time/s
15	90	0.75	
15	30	0.75	60
15	90	1	

3 Results and Discussion

3.1 Surface and cross-sectional morphology

Fig. 2 shows cross-sectional and surface morphologies of TTOs. The cross-sectional morphology of the TTOs shows that the coating grows in a single-layer structure, and the TTOs are uniformly bonded to the surface of the substrate. The TTOs show an obvious columnar growth structure during the growth process. In Fig.2a, the cross-section morphology of the S1 coatings shows a few microcracks. However, with the increase in Ti target power, the cross-section morphology of S2–S4 coating samples shows more closely packed columnar structure, as shown in Fig.2c–2d. This phenomenon is related to the diffusion energy of atoms. Studies have shown that substrate temperature, working pressure, sputtering power, and other parameters will affect the diffusion energy during atomic deposition, which in turn affects the microstructure of the coating[30]. In this study, the input power has a similar effect on the microstructure of the coating. In the deposition process of the S1 sample, the lower sputtering power causes insufficient diffusion energy for the sputtering atoms to migrate on the substrate surface, which leads to loose accumulation phenomenon and microcracks in the S1 coatings sample. On the contrary, in the S2–S4 samples with higher sputtering power, the sputtering atoms obtain enhanced atomic energy, enabling rapid diffusion and columnar growth at the initial deposition stage. Therefore, all TTO samples have no obvious cracks or only minimal defects, which indicates that the columnar structure is formed in a specific direction[31]. It can also be observed that the thickness of the coatings is uniform: S1, S2, S3 and S4 samples are measured to be 405.3, 403.1, 407.1 and 401.7 nm in thickness, respectively. The surface of the TTOs is smooth and dense, and free of

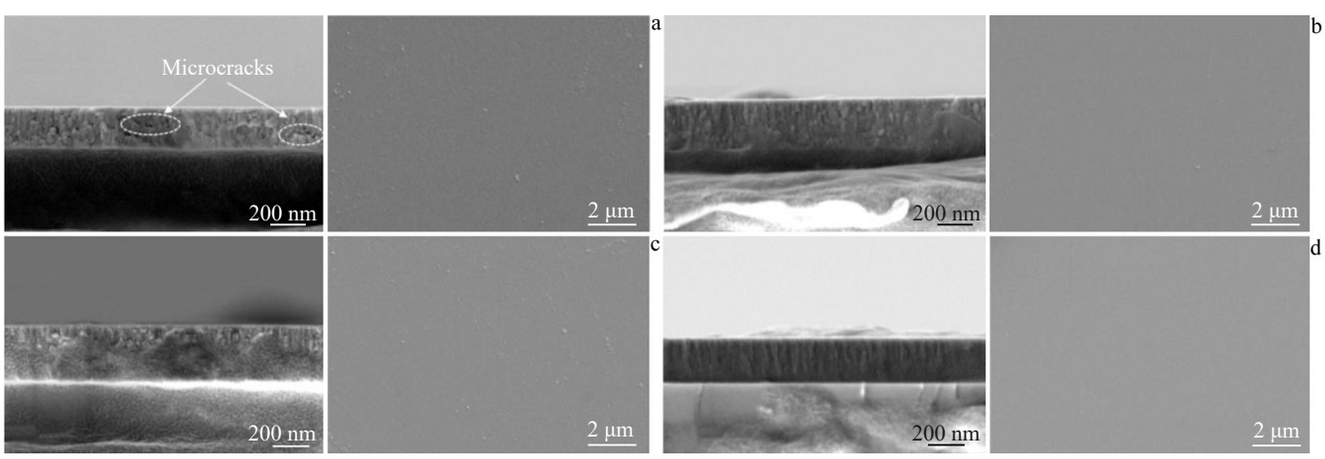

Fig.2 Surface and cross-section morphologies of TTOs samples: (a) S1, (b) S2, (c) S3, and (d) S4

microcracks or large voids. Due to the bombardment of high-energy particles, the mobility of adsorbed atoms during the growth of TTOs is improved, and the roughness, voids, and defects in the material are eliminated, thereby obtaining a smoother coating surface[32–33].

Fig. 3 shows typical TEM images of TTOs, through which the overall crystallinity and morphology of the TTOs were evaluated. Fig. 3a shows that the TTOs are stacked by layered structures during the deposition process. Fig. 3b and Fig. 3c show corresponding high-resolution image and selected area electron diffraction (SAED) pattern, respectively. Diffraction pattern in Fig.3c does not show clear lattice fringes, indicating that the phase structure of TTOs is mainly an amorphous phase.

3.2 Tribological properties

The friction and wear behavior of TTO samples on glass substrates were compared using a high-frequency linear super-slip tester. The SEM images of TTOs samples S1 – S4 after tribological testing are shown in Fig. 4. The wear track width was measured at least four locations. The wear track width of the TTOs sample S1 – S4 is 106±3 nm. SEM analysis reveals fractures and cracks along the edge of the wear track in all TTOs samples, as shown in Fig. 4a_1 – 4d_1. To study the wear behavior of TTOs in detail, the wear track was analyzed by

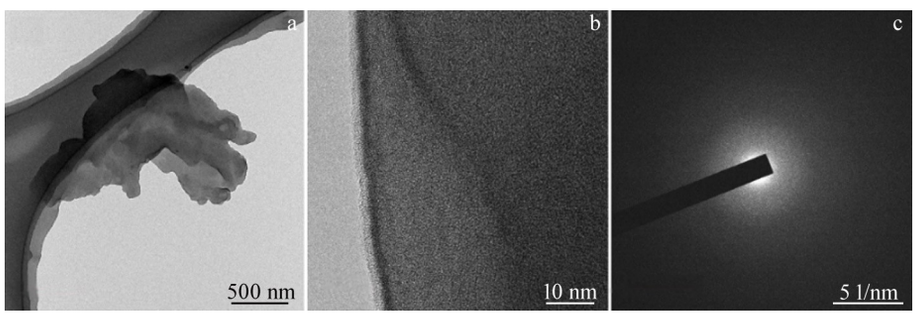

Fig.3 TEM images (a–b) and SAED pattern (c) of TTOs

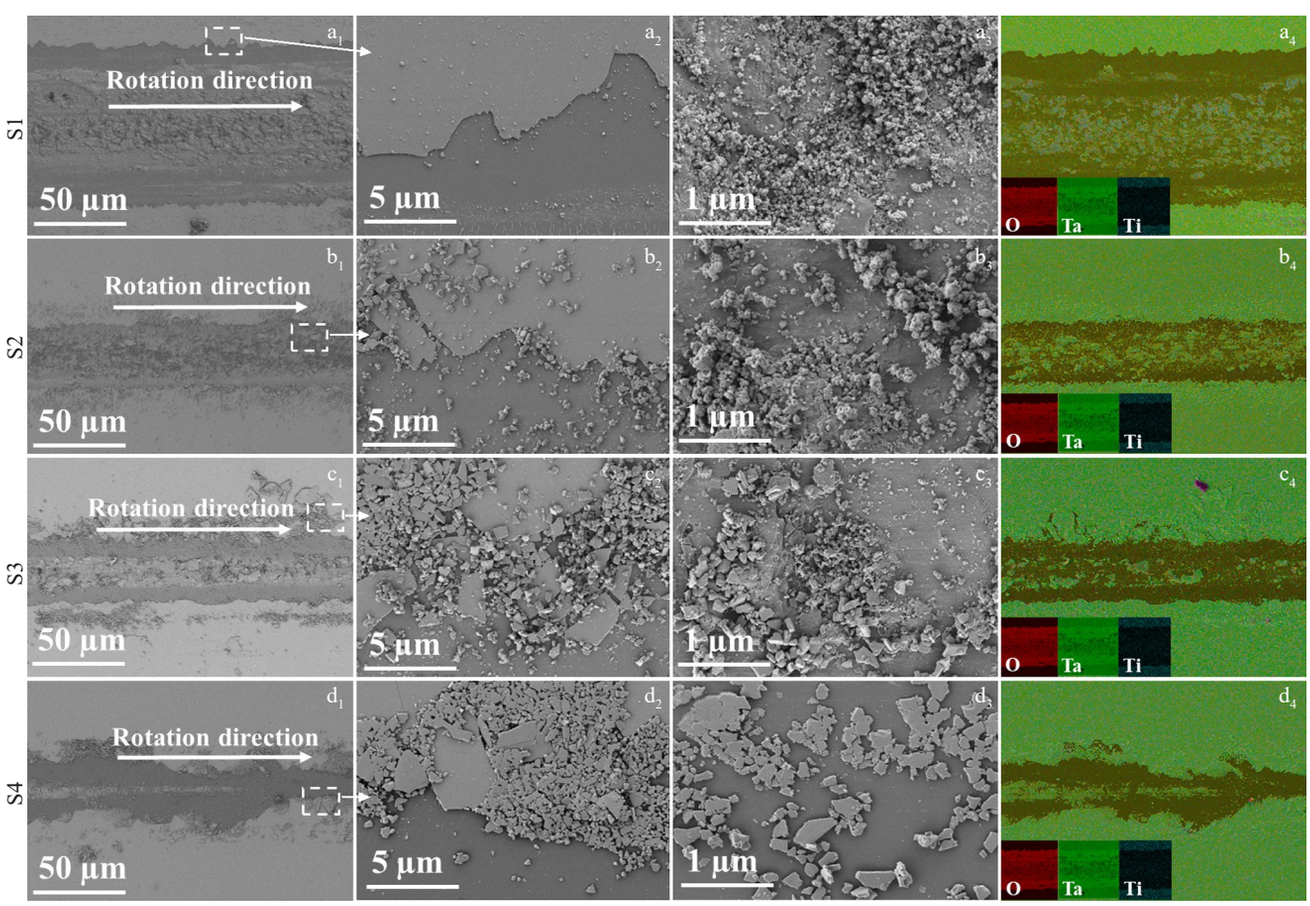

Fig.4 Friction and wear morphologies (a_1–a_3, b_1–b_3, c_1–c_3) and EDS mappings (a_4–d_4) of TTOs samples: (a_1–a_4) S1, (b_1–b_4) S2, (c_1–c_4) S3, and (d_1–d_4) S4

SEM, and the element mapping and quantitative composition analysis of the S1 coating sample were conducted by EDS. Results indicate severe surface damage to the TTOs after friction and wear testing. It can be see that the elements are evenly distributed in the coating.

Fig. $4a_1$–$4a_3$ and Fig. $4b_1$–$4b_3$ show that spalling and partial cracks appear in the friction contact area of TTO samples S1 and S2, respectively. The spalling morphology is mainly granular structure, and some smaller particle debris is compacted to form a protective coating in the wear area. The friction layer is formed by material transfer, wear traces, and cracks that pass through all layers[34]. Fig. $4c_1-4c_3$ and Fig. $4d_1-4d_3$ show that the spalling area of the friction contact area of the TTO samples S3 and S4 increases. The spalling morphology is mainly characterized by a mixed structure of small fragments and fine particles. The TTOs samples S3 and S4 have higher cohesion, thus improving the surface plasticity. The friction layer is formed by debris generated during sliding contact tests, which presses the wear area through reciprocating motion[35]. The TTOs are mainly characterized by plastic deformation and microcrack wear mechanism. Further analysis of Fig. $4a_4$–$4d_4$ shows that the content of Ta and Ti atoms in the selected friction layers of S1 and S2 samples is higher than that of S3 and S4 samples. Therefore, it is considered that the TTO samples S1 and S2 have stronger wear resistance.

3.3 Erosion performance and mechanism analysis

According to the erosion test parameters in Table 2, the simulated particle erosion test of TTOs was conducted. Fig.5a–5f are the erosion damage domain diagrams of the surface of the S1 and S2 samples after the erosion test. Compared with the surface morphology of TTO in Fig.2, the surface of S1 and S2 samples is smooth and flat before the erosion test. After the erosion test, the surface of the TTOs is broken, and the number of cracks and pits gradually increases with the extension of the erosion time. The S1 coating sample shows more pronounced plastic deformation and a more complex situation. Fig. 5g shows that the erosion damage area of S1 sample is larger than that of S2 sample under the same erosion parameters, which may be related to the differences in hardness and elastic modulus of the coatings. The ratios of hardness to elastic modulus (H/E) and hardness cubed to elastic modulus squared (H^3/E^2) are parameters reflecting a materials' resistance to plastic deformation, which are usually used to evaluate the toughness and wear resistance[36–37]. The variations of H/E and H^3/E^2 of samples S1 and S2 are shown in Fig.6. Notably, the sample S2 exhibit higher H/E and H^3/E^2 values than sample S1[21]. High hardness, toughness, and resistance to plastic deformation can reduce the peak impact force and energy absorption of coatings during erosion[38], explaining the superior erosion resistance of S2.

The micro-morphology of the TTO material surface after erosion was analyzed to study the variation of erosion resistance of TTOs under different erosion parameters. Fig. 7 shows the surface erosion morphologies of TTOs after tests with different erosion parameters. The erosion morphology shows that a large number of impact pits can be observed in

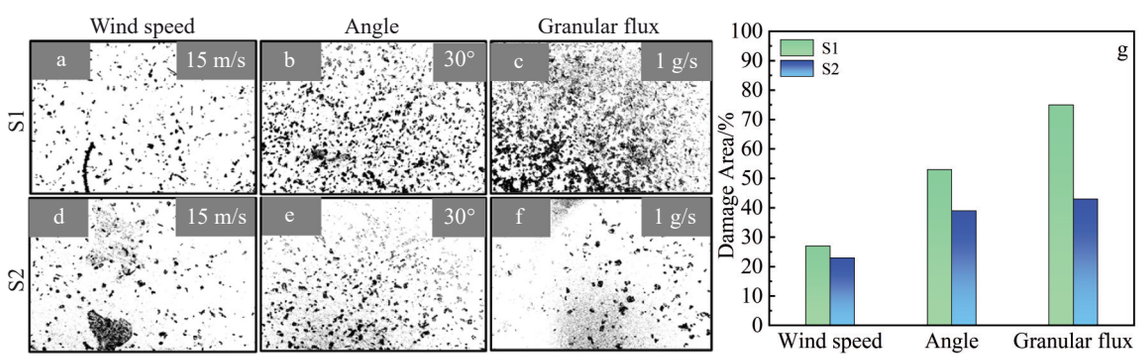

Fig.5 Erosion damage domain diagrams (a–f), and relationship between surface damage area and erosion parameters (g) of TTOs

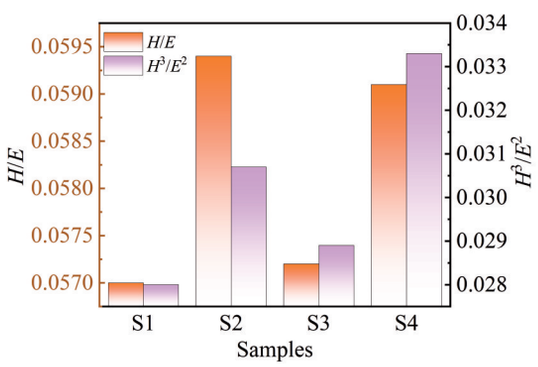

Fig.6 Variation of H/E and H^3/E^2 of samples S1–S4

the damaged area of the coatings, which are caused by the continuous impact of sharp particles[38]. Due to the low toughness of the TTOs, they cannot resist the high-energy impact of hard-corner particles and exhibit brittle spalling. Different surface erosion morphologies correspond to different damage forms of coating materials during the erosion process, which can reflect the erosion wear mechanism of TTOs.

As shown in Fig.7, at a wind speed of 15 m/s, the surface of the TTOs is dominated by peeling erosion pits, with microcracks generated around the pits, as well as the accumulation of flaking debris and granular structures. Long strip-shaped cracks extend around the erosion pit. During the continuous particles impact, large-area peeling of the TTOs

occurs[39]. The erosion wear mechanisms of TTOs primarily involve stress fatigue fracture wear and brittle fracture wear.

As shown in Fig. 8, at a 30º erosion angle, the micro-morphology of TTOs after the erosion test changes significantly. When the particle erosion angle is low, the damage area of TTOs expands. The surface damage form of TTOs after the erosion test is mainly the cutting and scratching of particles on the coatings.

As shown in Fig. 9, when the particle flow rate is 1 g/s, the micromorphology of TTOs after the erosion test is more complex and diverse. With the increase in particle flow rate, the impact frequency of TTOs increases significantly. The microstructure after the erosion test shows that many cracks and deep erosion pits appear in the erosion area of TTOs. Under the micro-cutting action of the corrosive medium, the TTOs continuously fall off, forming irregular spalling. Under the action of erosion particles, the spalling debris reattaches to the unpeeled coating[40].

Fig. 10 shows the microstructure and EDS elemental mappings of the surface of TTOs after the erosion test. There is no obvious element aggregation on the surface of TTOs after the erosion test. The contents of elements Ti, Ta, and O are 4.3%, 74.38%, and 21.31%, respectively. The element distribution on the erosion surface of TTOs plays an important

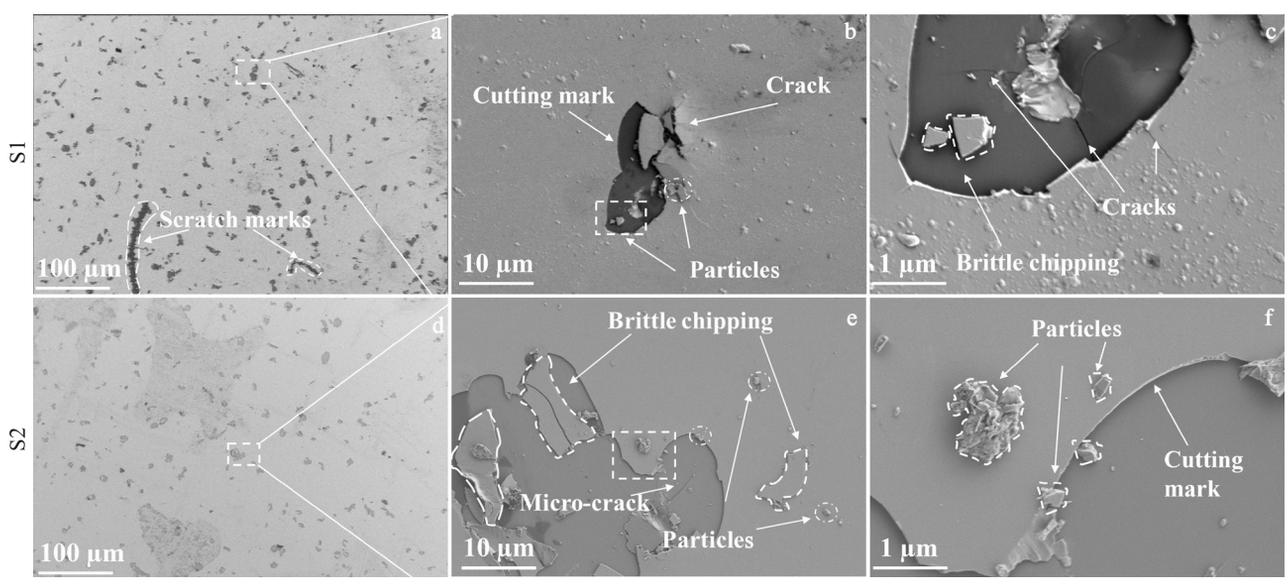

Fig.7 Erosion damage morphologies of TTOs at the wind speed of 15 m/s (Fig.7c and 7f are magnified images of dotted boxes marked in Fig.7b and 7e, respectively)

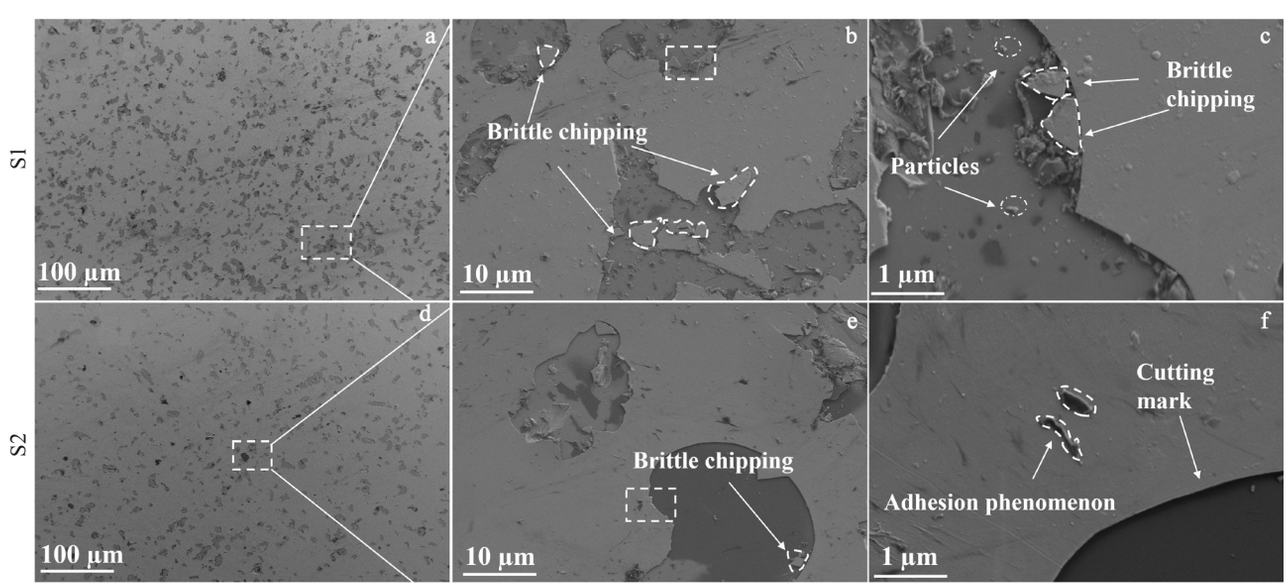

Fig.8 Erosion damage morphologies of TTOs at an erosion angle of 30° (Fig.8c and 8f are magnified images of dotted boxes marked in Fig.8b and 8e, respectively)

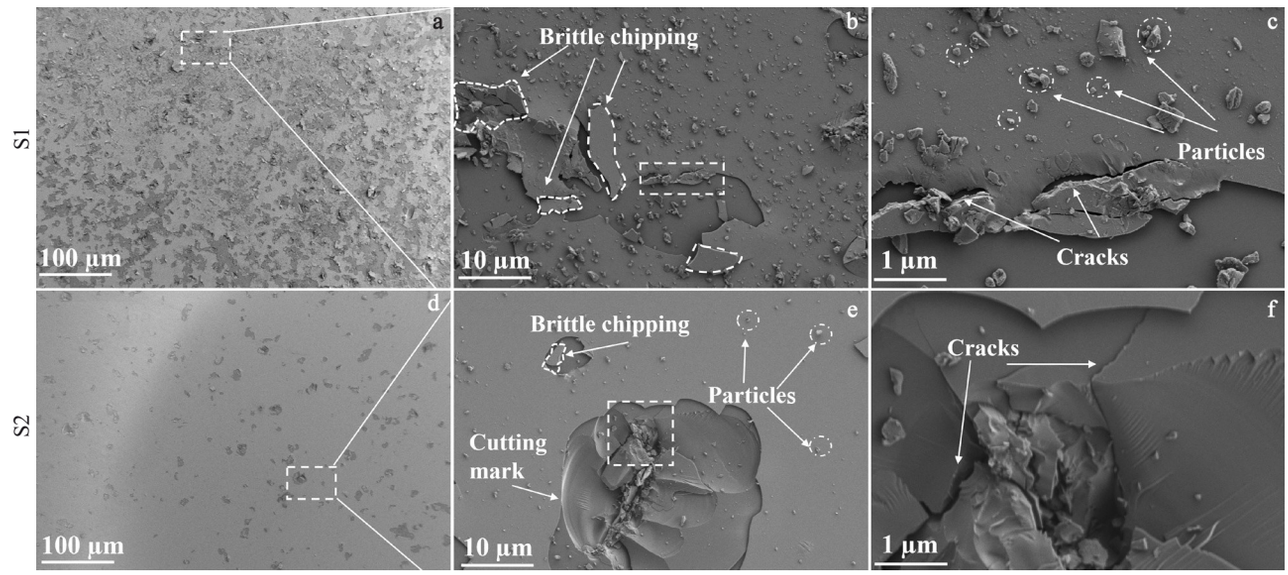

Fig.9 Erosion damage morphologies of TTOs at particle flow rate of 1 g/s (Fig.9c and 9f are magnified images of dotted boxes marked in Fig.9b and 9e, respectively)

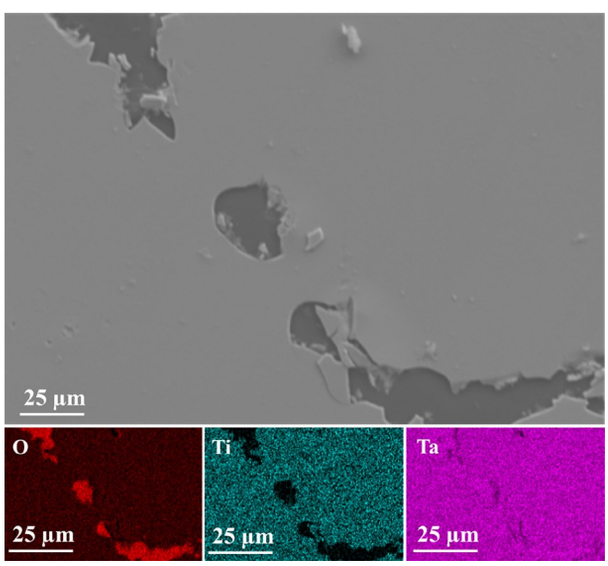

Fig.10 SEM image and EDS elemental mappings of TTOs erosion center area

role in revealing the erosion wear mechanism of the coatings, and has certain guiding significance for the design of anti-erosion materials.

The plasticity index (H^3/E^2) is a parameter to describe the resistance to plastic deformation of the coating, and the H^3/E^2 ratio is often used to simply describe the fracture toughness of the solid coatings. Finally, the plasticity indexes of various coatings under different working conditions are listed and analyzed, as shown in Table 3. To address the vulnerability of aircraft engine blades to sand-dust erosion damage, Cao[41] and Li[42] et al prepared TiN and AlCrN coatings on the surface of titanium alloy and evaluated their sand-dust erosion resistance using an erosion test platform. It

Table 3 H/E and H^3/E^2 of different types of erosion-resistant coatings

Sample	H/E	H^3/E^2
Ti-Ta_2O_5	0.0594	0.0307
TiN	0.0592	0.0799
AlCrN	0.0878	0.1790
Ti_2AlC	0.0583	0.0380

is found that both TiN and AlCrN coatings can improve the particle erosion resistance of titanium alloy substrate. The erosion wear characteristics of the coating surface mainly include micro-cutting marks, large particle plastic deformation, and spalling pits. During the erosion test, the coatings exhibit both plastic and brittle erosion wear mechanisms. Naveed et al[26] studied the effect of Ti_2AlC MAX phase coating on the erosion resistance of Ti6242 alloy. The heat treatment of Ti6242 alloy transformed the equiaxed microstructure into a dual-phase structure, thereby inducing a notable enhancement in surface hardness. With the increase in hardness, the improvement of erosion behavior is observed. Comparative analysis reveals that the erosion behavior can be predicted by estimating the value of H^3/E^2. Improving the plasticity index of the coatings can improve the erosion resistance of the coatings.

4 Conclusions

1) By tailoring the sputtering power of the Ti target, the microstructure of TTOs can be modulated, thereby inducing distinct variations in their mechanical properties. Finally, it has a key impact on the friction and wear characteristics and erosion resistance of the TTOs.

2) With the introduction of element Ti, the wear resistance of single Ta_2O_5 coatings is improved. When the sputtering

power of the Ti target is 30 and 40 W, the TTOs exhibit excellent mechanical and tribological properties. The simulated particle erosion test reveals that sample S2 has the best erosion resistance.

3) Microstructural characterization of TTOs after erosion testing reveals that their failure mechanism under erosive conditions involves impact forces from erodent particles, inducing extensive cracks in the coatings, and brittle spalling caused by crack propagation.

References

1 Chen Leihao, Dong Yiwei, Yang Hongwei *et al. Rare Metal Materials and Engineering*[J], 2024, 53(1): 281 (in Chinese)

2 Yeligeti M, Hu W, Scholz Y *et al. Environmental Research Letters*[J], 2023, 18(5): 054027

3 Jacobson M Z, Delucchi M A. *Energy Policy*[J], 2011, 39(3): 1154

4 Comello S, Reichelstein S, Sahoo A. *Renewable and Sustainable Energy Reviews*[J], 2018, 92: 744

5 Hu M J, Song X Y, Bao Z X *et al. Energies*[J], 2022, 15(17): 6408

6 Zakeri B, Paulavets K, Barreto-Gomez L *et al. Energies*[J], 2022, 15(17): 6114

7 Farghali M, Osman A I, Mohamed I M A *et al. Environmental Chemistry Letters*[J], 2023, 21(4): 2003

8 Zambrano D F, Villarroel R, Espinoza-González R *et al. Solar Energy Materials and Solar Cells*[J], 2021, 220: 110841

9 Said S A M, Walwil H M. *Solar Energy*[J], 2014, 107: 328

10 Jiang H, Lu L, Sun K. *Atmospheric Environment*[J], 2011, 45(25): 4299

11 Xu L Y, Li S Y, Jiang J M *et al. Solar Energy*[J], 2020, 199: 491

12 Yilbas B S, Ali H, Khaled M M *et al. Scientific Reports*[J], 2015, 5(1): 15833

13 Pop S C, Abbaraju V, Brophy B *et al. 2014 IEEE 40th Photovoltaic Specialist Conference (PVSC)*[C]. Colorado: IEEE, 2014

14 Humood M, Beheshti A, Meyer J L *et al. Tribology International*[J], 2016, 102: 237

15 Zambrano-Mera D F, Espinoza-Gonzalez R, Rosenkranz A *et al. Solar Energy Materials and Solar Cells*[J], 2023, 250: 112079

16 Ayadi A, Bouaouadja N, Durán A *et al. Ceramics International*[J], 2020, 46(8, Part A): 10634

17 Sansom C, Comley P, King P *et al. Energy Procedia*[J], 2015, 69: 198

18 Karim M, Naamane S, Delord C *et al. Solar Energy*[J], 2015, 118: 520

19 Beattie N S, Moir R S, Chacko C *et al. Renewable Energy*[J], 2012, 48: 448

20 Boyle L, Flinchpaugh H, Hannigan M. *Aerosol Science and Technology*[J], 2016, 50(4): 380

21 Chao Rui, Cai Haichao, Li Hang *et al. Optical Materials*[J], 2024, 147: 114680

22 Hegazy A A. *Renewable Energy*[J], 2001, 22(4): 525

23 Todt J, Pitonak R, Köpf A *et al. Surface and Coatings Technology*[J], 2014, 258: 1119

24 Azadi M, Rouhaghdam A S, Ahangarani S *et al. Surface and Coatings Technology*[J], 2014, 245: 156

25 Zhang H Z, Li Z Q, Ma C S *et al. Ceramics International*[J], 2019, 45(8): 10819

26 Naveed M, Renteria A F, Nebel D *et al. Wear*[J], 2015, 342–343: 391

27 Zambrano-Mera D F, Espinoza-González R, Villarroel R *et al. Solar Energy Materials and Solar Cells*[J], 2022, 243: 111784

28 Wiesinger F, Vicente G S, Fernández-García A *et al. Solar Energy Materials and Solar Cells*[J], 2018, 179: 10

29 Chao R, Cai H C, Li H *et al. Rare Metal Materials and Engineering*[J], 2024, 53(6): 1574

30 Yang Y H, Chen D J, Wu F B. *Surface and Coatings Technology*[J], 2016, 303: 32

31 Kaya E, Ulutan M. *Ceramics International*[J], 2022, 48(15): 21305

32 Zin V, Montagner F, Deambrosis S M *et al. Materials*[J], 2022, 15(9): 3354

33 Kubart T, Gudmundsson J T, Lundin D. *6 - Reactive High Power Impulse Magnetron Sputtering*[M]. Amsterdam: Elsevier, 2020: 223

34 González-Sevilla J E, Berumen J O, Flores-Martínez M *et al. Wear*[J], 2022, 498–499: 204337

35 Navarro C H, Martínez M F, Carvajal E E C *et al. The International Journal of Advanced Manufacturing Technology*[J], 2021, 117(5): 1565

36 Yang Shasha, Yang Feng, Chen Minghui *et al*. *Acta Metallurgica Sinica*[J], 2019, 55: 308 (in Chinese)

37 Xu S, Xu J, Munroe P *et al. Scripta Materialia*[J], 2017, 133: 86

38 Wang S G, He W F, Zhang H H *et al. Thin Solid Films*[J], 2023, 770: 139757

39 Yang Q, Mckellar R. *Tribology International*[J], 2015, 83: 12

40 Cai X J, Gao Y, Cai F *et al. Applied Surface Science*[J], 2019, 483: 661

41 Cao Xin, He Weifeng, He Guangyu *et al*. *China Surface Engineering*[J], 2016, 29(4): 60 (in Chinese)

42 Li J J, Wu F F, Wu B. *China Surface Engineering*[J], 2019, 48(2): 152 (in Chinese)

Ti掺杂Ta_2O_5高透光涂层抗冲蚀性能及损伤演变

晁　瑞[1,2]，叶博瑞[3]

(1. 河南科技大学 机电工程学院，河南 洛阳 471003)

(2. 河南省机械设计及传动系统重点实验室，河南 洛阳 471003)

(3. 合肥工业大学 机械工程学院，安徽 合肥 230009)

摘　要：为了验证Ti掺杂Ta_2O_5涂层（TTO）的耐磨特性和抗冲蚀性能，采用磁控溅射技术并通过控制Ti靶功率制备了一系列TTO涂层。研究了TTO涂层在不同Ti靶功率下的生长结构、组织形貌及摩擦学特性。冲蚀试验后，进一步分析了TTO涂层在不同冲蚀条件下，冲蚀损伤行为随力学特性的变化规律。结果表明，TTO涂层在生长过程中由于吸附原子的迁移消除了材料中的粗糙度、空隙和缺陷，获得了平整致密的光滑表面。摩擦学试验表明，TTO涂层主要表现为塑性变形和微裂纹的磨损机制。较高的Ti靶功率可以提升TTO涂层的耐磨性。冲蚀试验结果表明，冲击坑、犁沟、微切削、脆性剥落和裂纹的形成为TTO涂层样品在冲蚀作用下的主要磨损机制。

关键词：Ti-Ta_2O_5涂层；组织结构；摩擦学特性；冲蚀行为；损伤规律

作者简介：晁　瑞，男，1995年生，博士生，河南科技大学机电工程学院，河南 洛阳 471003，E-mail：chaoruibr@163.com